

An Anti-Freezing, Ambient-Stable and Highly Stretchable Ionic Skin with Strong Surface Adhesion for Wearable Sensing and Soft Robotics

Binbin Ying, Ryan Zeyuan Chen, Runze Zuo, Jianyu Li, and Xinyu Liu*

Natural living systems such as wood frogs develop tissues composed of active hydrogels with cryoprotectants to survive in cold environments. Recently, hydrogels have been intensively studied to develop stretchable electronics for wearables and soft robots. However, regular hydrogels are inevitably frozen at the subzero temperature and easily dehydrated, and have weak surface adhesion. Herein, a novel hydrogel-based ionic skin (iSkin) capable of strain sensing is demonstrated with high toughness, high stretchability, excellent ambient stability, superior anti-freezing capability, and strong surface adhesion. The iSkin consists of a piece of ionically and covalently cross-linked tough hydrogel with a thin bioadhesive layer. With the addition of biocompatible cryoprotectant and electrolyte, the iSkin shows good conductivity in wide ranges of relative humidity (15–90%) and temperature (−95–25 °C). In addition, the iSkin can adhere firmly to diverse material surfaces under different conditions, including cloth fabric, skin, and elastomers, in both dry and wet conditions, at subzero temperature, and/or with dynamic movement. The iSkin is demonstrated for applications including strain sensing on both human body and winter coat, human–machine interaction, motion/deformation sensing on a soft gripper and a soft robot at extremely cold conditions. This work provides a new paradigm for developing high-performance artificial skins for wearable sensing and soft robotics.

1. Introduction

Natural living systems display complex structures to survive in complicated and diverse environments. For example, properties such as freeze tolerance, dehydration resistance, and self-adaptation are commonly found in certain mammals, fishes, frogs, insects, and bacteria. For humans, skin is the largest organ of the body, serving as the first physical, thermal, and hygroscopic barrier to protect the inner body, maintain the body temperature and control transepidermal water exchange. The skin also contains the largest sensor network to perceive various environmental stimuli that humans encounter, such as pressure, strain, deformation, humidity, temperature, and pain. These functions are linked with salient features of the skin: highly deformable polymer networks (collagen and elastic fiber) to resist physical damage;^[1] hygroscopic compositions (e.g., pyrrolidone carboxylic acid) to retain water;^[2] fat cells to tolerate freeze; a variety of sensory neurons (e.g., mechanoreceptors, thermoreceptors, and nociceptors) to

transduce stimuli based on the controlled movements of inorganic ions (Figure 1A).^[3–5]


Many features of the human skin have inspired researchers to develop its electronic counterpart (i.e., artificial skins),^[6–10] leading to a variety of promising applications such as wearable electronics, wearable robotics, and soft robotics.^[11] Noticeably, because of the inherent material match and functional complementarity between artificial skins and soft robots, there have been significant research efforts spent on developing skin-like stretchable and wearable sensors for integration with various soft robotic systems.^[12–17] This rapid development would enable soft robots to interact with their users and environments more intelligently. Among different types of sensing materials used in artificial skins, hydrated and ionic materials such as deformable and tough ionic hydrogels are one of the most suitable sensor candidates to mimic the multiple functions of biological systems. Ionic hydrogels contain mobile ionic charge carriers replicating ion transport in the natural skin, and have excellent material biocompatibility,^[18–20] and tunable mechanical properties with on-demand design of toughness, stretchability,

Dr. B. Ying, R. Z. Chen, R. Zuo, Prof. X. Liu
Department of Mechanical and Industrial Engineering
University of Toronto
5 King's College Road, Toronto, Ontario M5S 3G8, Canada
E-mail: xyliu@mie.utoronto.ca

Dr. B. Ying, Prof. J. Li
Department of Mechanical Engineering
McGill University
817 Sherbrooke Street West, Montreal, QC H3A 0C3, Canada
Prof. J. Li

Department of Biomedical Engineering
McGill University
3775 rue University, Montreal, QC H3A 2B4, Canada

Prof. X. Liu
Institute of Biomedical Engineering
University of Toronto
164 College Street, Toronto, ON M5S 3G9, Canada

 The ORCID identification number(s) for the author(s) of this article can be found under <https://doi.org/10.1002/adfm.202104665>.

DOI: 10.1002/adfm.202104665

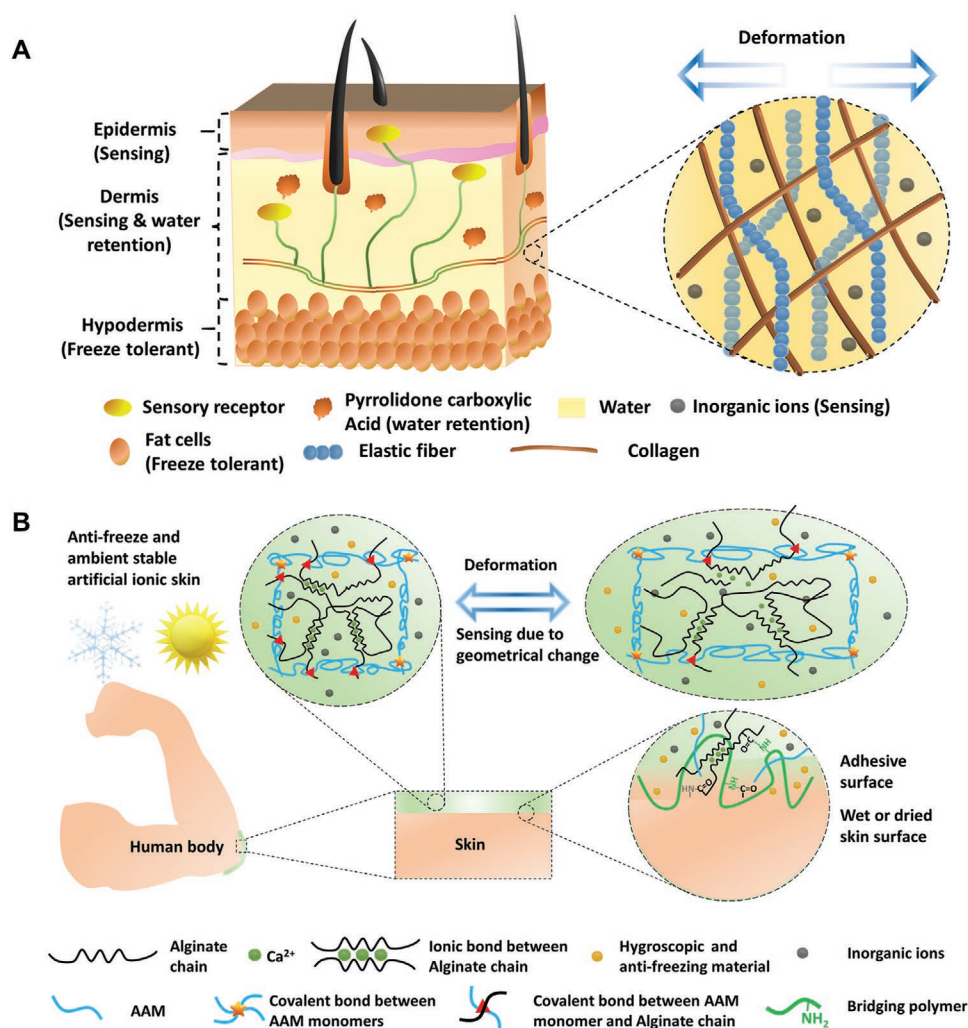


Figure 1. Design of a highly stretchable, anti-freezing and ambient-stable, artificial ionic skin (iSkin) with diverse strong adhesive capability. A) Schematic of the human skin that resists physical deformation due to the elastin fiber and collagen in the dermis layer, maintains the body temperature due to the fat cells in hypodermis layer, holds water due to the hygroscopic substance (i.e., pyrrolidone carboxylic acid), and transduces stimuli due to the controlled movements of inorganic ions. B) Schematic illustration of an iSkin adhered to diverse substrates (the human skin is used here as an example). The iSkin is made from a hydrogel dissipative matrix (light green circle) containing both ionically (calcium; green circles) cross-linked and covalently cross-linked polymers (black and light blue lines) and is laden with hygroscopic and anti-freezing reagents (yellow circles) and inorganic ions (gray circles). The iSkin surface consists a layer of bridging polymer with plenty of primary amines (green lines), which can penetrate the iSkin and the target substrate.

and elasticity to accommodate the diverse mechanical properties of surfaces the artificial skin will be mounted on.^[21,22] Recently, a variety of ionic hydrogel-based, skin-like devices (also called hydrogel-based iontronic devices) have been developed, including pressure sensors,^[8,23] touchpads,^[10,24] strain sensors,^[10] and robotic skins.^[12] These devices are capable of transducing applied touch, pressure, deformation, humidity, or temperature into changes of electrical signals (e.g., capacitance or resistance), and mimicking the sensing functions of natural skin.

Despite the recent advances, researchers still need to address several important challenges to further broaden the practical applications of hydrogel-based iontronics. For instance, ionic hydrogel-based devices must possess long-term stability

(i.e., by mitigating water loss) during open-air operation, and simultaneously maintain mechanical deformability and electrical conductivity in cold environments (i.e., anti-freezing characteristics). Without special material design, water evaporation and freezing significantly weaken the mechanical and electrical properties of hydrogels. Thus, the real-world sensing application of ionic hydrogels is still limited by their poor ambient stability. In addition, for many applications such as wearable sensing and soft robotics, ionic hydrogel-based devices should firmly adhere to substrates of different materials (e.g., human skins, fabric clothes, and elastomers) under various conditions (e.g., dry and wet surfaces, sweaty skin, subzero temperature, and dynamic deformation and movement) to enhance the fidelity of signals acquisition, and show good biocompatibility

Table 1. Comparison between the iSkin and other similar hydrogel devices reported previously (RT: room temperature; PEDOT:PSS: Poly(3,4-ethylenedioxythiophene) polystyrene sulfonate; ILs: ionic liquids; G: glycerol; MAANA: sodium methacrylate; SC: sodium casein; Na₃Cit: sodium citrate).

Strain _{max} (RT)	Toughness _{Fracture} (J m ⁻² , RT)	Reported anti-freezing capability [°C]	Conductivity [RT, S m ⁻¹]	Ambient stability	Adhesion capability	Solvent	Electrolyte salt/conductor	Bio-toxicity ^{b)}	Refs.
1973%	11 410	−95	0.9	≥30 d	649 J m ⁻² (Both wet and dry)	H ₂ O, G	NaCl	Low	This work
700%	2000	−57	8	N/A	No	H ₂ O	CaCl ₂	N/A	[49]
620%	2300	−20	8.2	≥30 d	60 kPa (Dry)	H ₂ O, G	CNT	High	[35]
1700%	N/A	−40	1.928 × 10 ⁻⁴	≥ 2 d	No	H ₂ O, EG	NaCl	High	[66]
300%	N/A	−40	1.6	N/A	No	H ₂ O, EG	LiCl	High	[67]
1390%	N/A	−75	0.83	N/A	No	H ₂ O	ILs	High	[68]
2100%	N/A	N/A	0.35	No	250 J m ⁻² (Wet)	H ₂ O	SC	Low	[69]
2000%	N/A	−20	1.5	No	40 J m ^{-2a)} (Dry)	H ₂ O, G	MAANA	N/A	[70]
960%	N/A	−55	N/A	N/A	No	H ₂ O, EG	PEDOT:PSS	N/A	[71]
960%	N/A	−80	N/A	≥7 d	≈100 kPa (Dry)	H ₂ O, G	Na ₃ Cit	N/A	[72]
≈600%	N/A	−24.7	0.72	N/A	No	H ₂ O	NaCl	Low	[73]
400%	N/A	−80	0.765	>30 d	No	H ₂ O, G	KCl	Low	[74]
900%	N/A	−20	1.1	N/A	No	H ₂ O	ILs	High	[75]
715%	N/A	−20	0.4	N/A	No	H ₂ O, G	NaCl	Low	[76]

^{a)}Calculated as force/width curve in the paper; ^{b)}Biocompatibility and comfortability for on-skin usage.

when interfacing with human body. Conventional hydrogel devices and most electronic skins usually do not have good self-adhesion and therefore can only adhere to substrates with the assistance of additional adhesives such as bandages, scotch tapes, or 3M adhesives.^[25–27] However, these adhesives can easily debond when adhering to substrates under certain conditions such as wet, cold, and continuously deformed surfaces; they are not suitable for use under subzero temperatures due to the hardening of adhesive matrix; the limited biocompatibility of some of these adhesives could be another issue when used for wearable devices on human body. To date, there are no existing hydrogel-based devices that can satisfy the aforementioned requirements simultaneously (previous reports summarized in Table 1).

To address these challenges, we report a new design of hydrogel-based ionic skin (iSkin) recapitulating the salient features of human skin, which possesses high stretchability, high toughness, good long-term ambient stability, superior anti-freezing property, and strong surface adhesion to different types of surfaces. The unique combination of these properties enables a variety of applications of the iSkin to wearable sensing and soft robotics. The experimental results demonstrate that the iSkin has a rupture toughness of 11.41 kJ m⁻², sustains more than 1975% strains without rupture, and maintains its electrical function after 1300 cycles of stretching deformation. As a sensor, the iSkin shows a comparable conductivity (0.904 S m⁻¹) to similar ionic conductive hydrogels under ambient conditions of the laboratory environment (21 °C and relative humidity of 60–65%). In addition, it can maintain its conductive property for at least one month in the laboratory environment. With extreme low-temperature tolerance (down to −95 °C), the iSkin shows an acceptable level of conductivity (1.96 × 10⁻⁵ S m⁻¹) for sensing even at −70 °C. As a promising sensor candidate for smart clothes, wearables and soft robotics at various extreme

environment conditions, the iSkin can strongly adhere to different substrate surfaces (i.e., elastomer and cloth fabric with an adhesion energy of 398 J m⁻², dry and sweaty skin surfaces with an adhesion energy of 649 J m⁻²) to ensure secured attachment and sensing signal fidelity. In addition, the adhesion of the iSkin on various surfaces shows excellent long-term stability both in water environment and at subzero temperatures (tested at −30 °C). These merits of the iSkin could potentially blur the boundary between humans and machines, and promise broad applications such as strain-sensing smart clothes in wet, underwater, and/or extremely cold conditions, fabric-hydrogel hybrid robotic exosuits for operation in harsh environments, smart sensing gloves for human–machine interaction, deformation/force-feedback soft robots for interactive manipulation and navigation.

2. Results

2.1. Design of the iSkin

The iSkin consists of two layers: i) a bulk dissipative hydrogel matrix containing hygroscopic/cryoprotective substances and inorganic ions; ii) an adhesive thin layer of an interpenetrating positively charged bridging polymer coated on the hydrogel surface (Figure 1B). The dissipative hydrogel matrix is composed of a tough double-network (DN) hydrogel containing hybrid cross-linked and interpenetrating alginate-polyacrylamide (Alg-PAAm) networks, and the selection of Alg and PAAm for constructing the tough hydrogel was due to their excellent mechanical performance capable of effectively dissipating energy under deformation,^[28] confirmed biocompatibility and wide use in biomedical devices.^[29–32] Cryoprotective solutions have been widely applied to prevent

various biological samples from icing damage at subzero temperatures, owing to their inhibition behaviors of hindering the ice crystallization of water molecules.^[33] Here, we incorporated glycerol, as a hygroscopic and cryoprotective material, into the tough hydrogel matrix to reduce the loss of water and lower the ice crystallization temperature of the hydrogel. We selected glycerol for this purpose because it is well accepted as a nontoxic anti-freezing, hygroscopic agent and a nonionic kosmotrope,^[34] which brings minimal impact to the mechanical performance of tough hydrogel as well as to the adhesive layer. The model inorganic ions used here are sodium (Na⁺) and chloride (Cl[−]) ions since sodium chloride (NaCl) is the most common electrolyte salt and shows low biotoxicity in noninvasive scenarios (e.g., epidermal wearable sensing and soft robotic sensing) and good electrical conductivity. After the tough hydrogel fully cross-linked (overnight at the room temperature), we incorporated the glycerol–water binary solvent (glycerol: 66.6 wt%) with saturatedly dissolved NaCl into the prefabricated tough hydrogel matrix by a facile method called solvent exchange for 2.5 h to ensure the full equilibrium state,^[33] in which the solvent solution volume is 20 times the volume of the hydrogel (see details in Figure S1A,B, Supporting Information and the Experimental section). During the solvent exchange process, the water molecules in the hydrogel were exchanged with the hygroscopic/cryoprotective molecules and the electrolyte ions. This process maintained the high transparency of the tough hydrogel (the iSkin in Figure S5C, Supporting Information). Compared with the previously demonstrated one-pot synthesis that introduces the binary solvent and electrolyte into the monomer solution during polymerization (ionic cross-linking of alginate network and covalent cross-linking of PAAm network),^[35] this two-step solvent exchange method avoids the complicated optimization process during synthesis. In addition, this method can be conveniently expanded to fabricate tough hydrogels incorporating a variety of cryoprotectant and electrolyte solutions at different concentrations, allowing the facile tuning of the anti-freezing property, conductivity, and mechanical properties (e.g., toughness and stretchability) of the material as needed.

We rendered the tough hydrogel surface highly adhesive by employing a bridging polymer that bears positively charged primary amine groups. Here, chitosan was selected as the bridging polymer because of its high concentration of primary amine groups and the resultant strong adhesion energy.^[29] Such a bridging polymer can be absorbed to a surface through both electrostatic attraction and covalent bonding. In terms of covalent bonding, the amide bond (−CO−NH−) can be formed between primary amine groups (−NH₂) on the bridging polymer and carboxylic groups (−COO[−]) on both the tough hydrogel matrix (mainly the alginate network) and the to-be-adhered substrate (e.g., skin, carboxylated elastomer, and carboxylated cloth fabrics) (Figure 1B) in the presence of two common coupling reagents [1-ethyl-3-(3-dimethylaminopropyl) carbodiimide (EDC) and N-hydroxysulfosuccinimide (NHS)]. In addition, carboxylic acid groups on the alginate network and primary amine groups on the to-be-adhered substrate (e.g., skin and aminated elastomer) can form the amide bond directly in the presence of EDC and NHS (Figure 1B). If the to-be-adhered substrate is permeable, the bridging polymer can penetrate into

the target surface (e.g., skin), forming physical entanglements and chemical anchors (Figure 1B).^[29] Our ready-to-use iSkin with adhesive was then applied on the to-be-adhered substrate with compression. We hypothesized that this unique material design converts the original water-based tough hydrogel into a cryoprotectant-based organohydrogel with increased freezing tolerance,^[33] high stretchability, high ambient stability, good conductivity, and strong adhesion on surfaces under diverse conditions (e.g., wet, cold, and dynamically deformed surfaces), making it feasible to construct the adhesive iSkin for use in various environments.

2.2. Mechanical and Electrical Testing of the iSkin

The mechanical performance of the iSkin was first tested at room temperature (21 °C). The pure-shear testing showed that the iSkin can be stretched to 1975% of its initial length without rupture (Figure 2A,B and Movie S1, Supporting Information), and the fracture energy (i.e., fracture toughness) was determined to be 11.4 kJ m^{−2} (Figure 2B,C and Figure S2A,B, Supporting Information). Adding glycerol and NaCl into the original tough hydrogel during iSkin preparation altered its mechanical properties. While exhibiting similar stretchability [1975% vs 2200% for the original one (Figure S3A and Movie S2, Supporting Information)], our iSkin displayed a slightly higher fracture toughness (11.4 kJ m^{−2}) and higher Young's modulus (53.6 KPa, Figure 2B) compared with the original tough hydrogel [fracture toughness: 9.3 kJ m^{−2} (Figure 2C, Figure S2C,D, Supporting Information) and Young's modulus: 26.2 KPa (Figure S3A, Supporting Information)]. The original Alg-PAAm tough hydrogel was formed by covalently and ionically cross-linked polymers. The electrostatic interactions between alginate chains and calcium ions formed ionic cross-links that unzip and can dissipate energy under deformation.^[36] Surprisingly, we found the monovalent ions (Na⁺ and Cl[−]) within the iSkin matrix did not impair the mechanical performance of the tough hydrogel, which is different from the results of a previous report.^[37,38] The enhancement of mechanical property after solvent exchange is possibly due to the incorporation of the glycerol–water binary solvent system. Glycerol introduced noncovalent interactions within the hydrogel polymer chains^[35] and increased the polymer network density,^[33] which was evidenced by the shrinkage of the hydrogel length measured by $6.2 \pm 2.5\%$ ($n = 3$) during solvent exchange. In addition, the incorporation of glycerol could possibly reduce the competition of the Na⁺ and Cl[−] ions for binding sites on the alginate chains, thus protecting the ionic cross-links.

To further verify this speculation, cyclic tensile testing of hydrogels with different synthesis conditions was carried out; all the testing results of the original tough hydrogel, glycerol-laden tough hydrogel, and iSkin revealed a large hysteresis loop in the first loading-unloading cycle (Figure S3B,C,F, Supporting Information), corresponding to the breakage of ionic cross-linking of the alginate network. Following the first cycle, these hydrogels became elastic due to the permanent cross-linking of the PAAm network (Figure S3B,C,F, Supporting Information). In contrast, both the glycerol-laden Alg-PAAm hydrogel without Ca²⁺ cross-linking and the iSkin without Ca²⁺ cross-linking

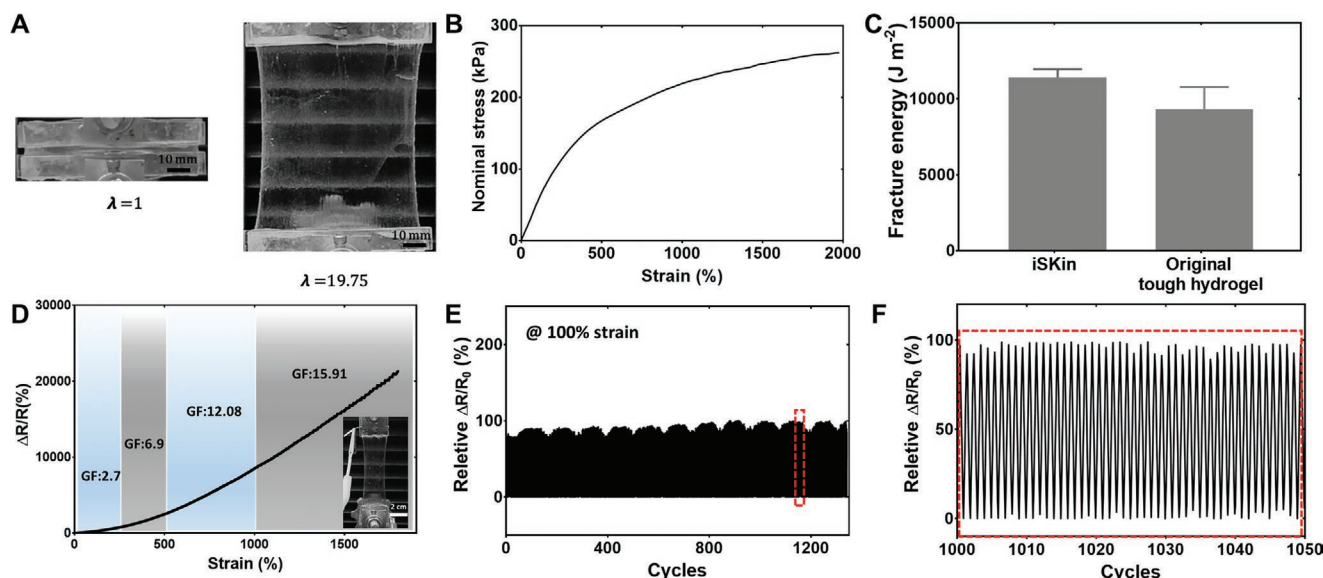


Figure 2. Mechanical and electrical testing of iSkin. A) iSkin was stretched to more than 1975% (right figure) of the original length (left figure) without fracture. B) Strain–stress curve of iSkin under stretch. C) The comparison of fracture toughness between iSkin and original Alg-PAAm tough hydrogel ($N = 4$ for iSkin and $N = 3$ for original tough hydrogel). D) Relative resistance change as a function of strain and its gauge factor (GF) at different strain ranges. The inset figure shows the resistance measurement setup during the tensile testing. E) Stability of relative resistance changes of iSkin at 100% strain for 1300 cycles. F) Zoom-in view of data in (E) from cycle 1000 to 1050. R_0 is the initial resistance value of each cycle. The overall time for the stability test is 7.5 h at the relative humidity (RH) of 25% under room temperature.

showed no obvious hysteresis loop during five continuous loading–unloading cycles (Figure S3D,E, Supporting Information). The disappearance of the hysteresis loop in testing results of the Ca^{2+} cross-linking-free hydrogel matrices further proved that the ionic cross-linking on the alginate chains is critical for the mechanical properties of the tough hydrogel, and that monovalent ions (Na^+ and Cl^-) within the iSkin hydrogel matrix have a negligible effect on the ionically cross-linked alginate chains due to the incorporation of glycerol. Furthermore, both the iSkin (with glycerol and NaCl electrolyte) and the glycerol-laden tough hydrogel (without NaCl electrolyte) showed higher elastic moduli [53.6 kPa for iSkin and 58.8 kPa for glycerol-laden tough hydrogel (Figure S3C, Supporting Information)] than that (26.2 kPa) of the original tough hydrogel. The increase in hydrogel Young's modulus after glycerol incorporation could be due to the reinforcement effect of the hydrogel matrix caused by noncovalent interactions (hydrogen bonds) between hydroxyl groups on the glycerol chains and carboxyl groups and amino groups on the alginate and PAAm chains.^[35] Consequently, the iSkin also showed an increased fracture toughness compared with the original tough hydrogel. Moreover, it is worth noting that there is a smoother elastic-to-plastic transition on the characteristic curve of the iSkin (Figure 2B) than that of the original tough hydrogel (Figure S3A, Supporting Information), which could be due to the large amount of noncovalent interactions between glycerol chains and alginate and PAAm chains (e.g., hydrogen bonds). The high stretchability ($\leq 1975\%$) of the iSkin can meet the mechanical requirements of wearable sensing and soft robotics given the typical strain levels of human skin during movements [$\leq 55\%$ ^[10]] and most soft robots [$\leq 100\%$ – 150% ^[39]]. The comparable mechanical performance (e.g., Young's module, toughness, or stretchability) of

the iSkin to that of other substrates (e.g., skin and elastomers) will make it a suitable material candidate for constructing sensors for wearables and soft robots.^[22,40]

The electrical characteristics of the iSkin were then examined at room temperature (21 °C). Stainless steel electrodes (0.02 mm thick) were used to establish electrical contacts on the hydrogel. Although the incorporation of glycerol enhanced the mechanical performance of tough hydrogel and its anti-freezing properties (to be discussed below), the addition of the organic solvent glycerol (66.6 wt%) significantly reduced the ionic hydrogel's conductivity (Figure S4A, Supporting Information). With the addition of NaCl, the conductivity of the glycerol-laden hydrogel was recovered and reached its maximum of $0.904 \pm 0.302 \text{ S m}^{-1}$ ($n = 4$) at NaCl's saturation concentration (5.4 M), more than twice the conductivity of original tough hydrogel (Figure S4A, Supporting Information). Further addition of NaCl into the solvent exchange solution for treating the hydrogel does not help because no more NaCl can be dissolved (Figure S4B,C, Supporting Information). We adopted this glycerol–water binary system with saturated NaCl for solvent exchange treatment of the hydrogel to achieve the highest conductivity, which is desired in sensing applications. The conductivity of the iSkin (0.904 S m^{-1}) is comparable to those of previously reported conductive ionic hydrogels (Table 1).

Taking advantage of its high stretchability and good conductivity, the iSkin can serve as a highly deformable and stretchable strain sensor. A representative plot of the relative resistance change ($\Delta R/R$) as a function of tensile strain of an iSkin sample ($L \times W \times T$: $5 \times 28 \times 1.4 \text{ mm}^3$, tensile direction: 5 mm edge) is presented in Figure 2D. It is observed that the resistance of the iSkin proportionally increases with the applied strain up to 1800%. To evaluate the strain sensitivity of

iSkin-based sensors, the gauge factor (GF) was further calculated from the slope of the relative resistance change ($\Delta R/R$) versus strain at different slope ranges. As shown in Figure 2D, the GF was found to increase with the strain. The resistance R is given by the equation $R = \rho l/A$, where ρ is the resistivity of the iSkin, l is the length, and A is the cross-sectional area of the iSkin. Note that the deformation of a hydrogel only changes the configuration of its polymer network and water molecules with negligible effect on its ionic conductivity. Upon stretching to λ times its original length, the cross-sectional area of ionic hydrogel is reduced by a factor of λ due to the material's incompressibility. As a result, the ratio of the resistance of the stretched hydrogel (R) to that of the unstretched hydrogel (R_0) is $R/R_0 = \lambda^2$. Accordingly, the GF is calculated as $(R-R_0)/[(\lambda-1) \cdot R_0] = \lambda+1$. For example, the average GF can reach to 6.9 once the strain range is from 250% to 500% and 15.91 from 1000% and 1800%, respectively. The maximum strain level and GF of the iSkin are comparable to those of previous reported organohydrogel or hydrogel-based strain sensors.^[41,42] Moreover, we experimentally determined the response time and recover time of the iSkin at low frequencies (<4 Hz) as current pneumatically actuated soft robots and wearable sensing typically work in the frequency less than 5 Hz.^[43] For example, the dynamic performance of the iSkin clearly shows the synchronization of deformation and measured resistance change at relevant mechanical frequencies (e.g., 1 Hz and 2 Hz, Figure S4D,E, Supporting Information). The response time can be characterized as 9 ms through a homemade step mechanical stretch loading test (Figure S4F, Supporting Information), which is close to the theoretical value of resistance-capacitance (RC) time constant (on the order of 10 ms) of hydrogel sensors. In addition, the durability of iSkin for strain sensing was also tested. After 1300 cycles of repeated tensile loading-unloading cycles, the relative resistance change was maintained well even at a dry laboratory condition (RH = 25%, Figure 2E,F), indicating its good retention of strain sensing function. The conductivity durability and the comparable strain sensitivity of the iSkin will make it a suitable sensing component for long-term use on wearables and soft robot.

2.3. Ambient Stability and Anti-freezing Testing of the iSkin

We next examined the effect of hygroscopic/cryoprotective substance on ambient stability and anti-freezing capability of the iSkin. Compared with other bioinspired neutral substances (e.g., ethylene glycol and dimethyl sulfoxide) and pure concentrated salts especially in high concentration (e.g., lithium chloride, sodium chloride, and calcium chloride),^[44] glycerol was selected here as the hygroscopic/cryoprotective candidate because of its low biotoxicity during on-skin wearable sensing, the little damage it causes on the ionic cross-linking network and charging groups within the adhesive layer due to the neutrally charged property of glycerol, and its effective anti-dehydration and freezing inhibiting effects by disrupting the hydrogen bonds between H_2O molecules^[33] and by forming strong hydrogen bonds with water molecules.^[45]

First, the changes in mass and resistance of iSkin samples ($L \times W \times T$: $40 \times 10 \times 1.4$ mm³) were characterized to

measure its ambient stability at room temperature under different humidity conditions. No mass decrease was observed on samples stored at the relative humidity (RH) of 63% over 30 d (Figure 3A). Interestingly, the iSkin stored in the high RH environment (RH = 88%) experienced a slight mass increase due to the large amounts of hydroxyl groups on the glycerol chains that led to a lower vapor pressure of water in the iSkin hydrogel matrix than the environment. In contrast, the mass of the original tough hydrogel rapidly decreased to 20% of the original mass, even in the extremely wet environment (RH = 88%) after only 3 d storage (Figure 3A and Figure S5A, Supporting Information). This large mass reduction is due to the fact that the original hydrogel matrix without glycerol has a higher internal vapor pressure of water than that of the environment.^[46] Noticeably, in an extremely dry environment (e.g., RH = 15%), the iSkin can still maintain 75% of its original mass even after 30 d (Figure 3A), validating the strong water-retaining capability of glycerol. Similarly, the electrical resistance (measured along its length direction) of the iSkin shows a good long-term ambient stability. For instance, there is no obvious resistance fluctuation observed on the iSkin device in the first 5 d while the resistance of the original tough hydrogel increased significantly even at the high RH conditions (RH = 63% and 88%, Figure 3B). On the other hand, although the resistance of the iSkin in an extremely dry environment (e.g., RH = 15%) experienced certain increase (because water evaporation increased the concentration of the polymer chains and reduced the ion mobility), the resistance level of ≈ 100 k Ω after 30 d storage can still meet the requirement of strain sensing.^[47] In addition, we also studied the ambient stability of pure NaCl-laden hydrogel. The hydrogels treated with pure saturated NaCl solution (5.4 m) showed relatively good stability in a humid environment (RH = 88%) but experienced obvious mass decreases of 33.2% and 57.1% after 30 d when the RH was 63% and 38%, respectively (Figure S5B, Supporting Information). In addition, the NaCl-laden hydrogel easily lost its high transparency for long-term storage even at RH = 63% because of salt precipitation as the evaporation of water from hydrogel (Figure S5C, Supporting Information). These findings further prove that pure salts (e.g., NaCl) are not sufficient to maintain the water content in the hydrogel and to enhance its ambient stability. In contrast, the iSkin maintained its optical transmittance and shape at RH = 63% after 30 d, while the original hydrogel shrunk obviously (Figure S5C, Supporting Information). These observations indicate that the iSkin can preserve its optical transparency, shape, and ion-based electronic function and could serve as a good ambient-stable material for many potential applications, particularly for wearable sensing and soft robotics during the open-air usage.

As a promising sensing unit for wearables and soft robots, we then examined the anti-freezing performance of the iSkin in subzero temperature environments. There are three different states of water in a hydrogel system, namely "free water" (fast exchange), "intermediate water" (slow exchange), and "unfrozen bound water."^[46] Here, glycerol (66.6 wt%) solution dissolved with saturated NaCl content was used to treat tough hydrogel to optimize its amount of unfrozen bound water and enhance its anti-freezing property.^[48] Indeed, the as-synthesized iSkin showed excellent freezing tolerance with good

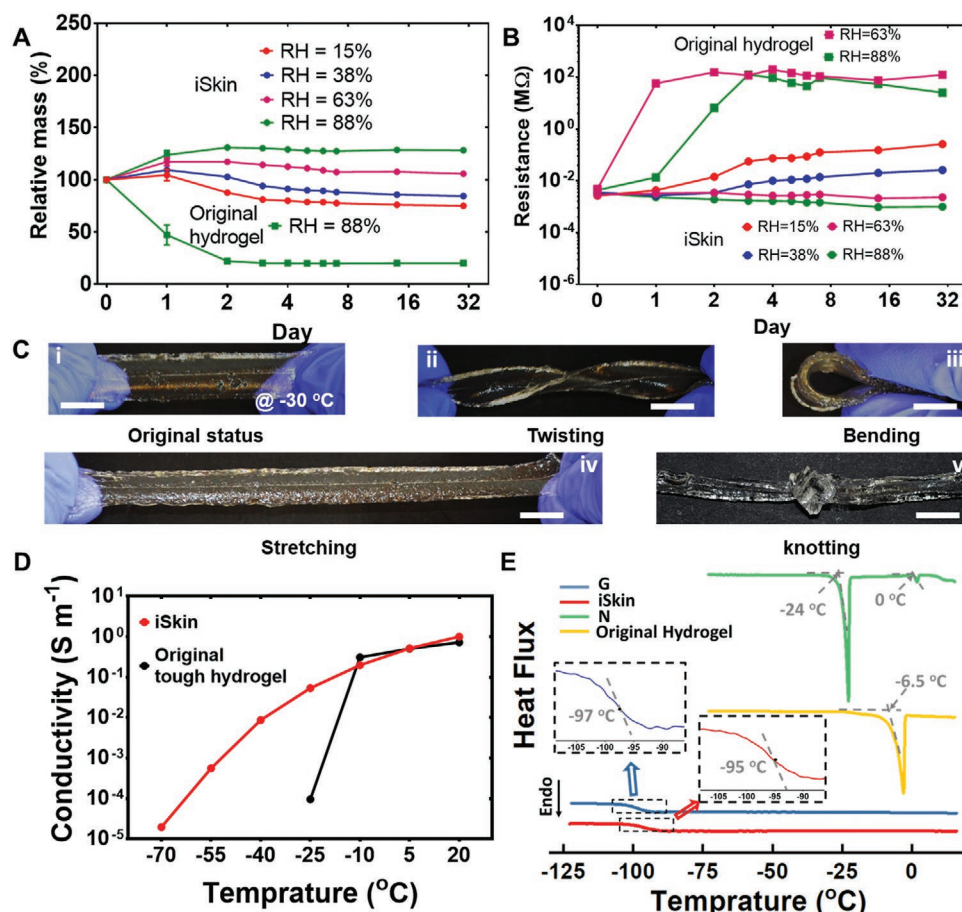


Figure 3. Ambient stability and anti-freezing capability of iSkin. A) Mass change as a function of RH (15%, 38%, 63%, and 88%) for iSkin within 30 d. Original Alg-PAAm tough hydrogel at the RH = 88% was used as control. The mass of hydrogel is normalized with its initial mass ($N = 4$). B) The resistance changes of iSkin and original Alg-PAAm tough hydrogel under different humidity conditions within 30 d. C) Photographs of iSkin without freezing, which can twist, bend, stretch and knot at $-30\text{ }^{\circ}\text{C}$. Scale bar: 2 cm. D) Temperature-dependent ionic conductivity investigation of iSkin and the original tough hydrogel. E) Dynamic scanning calorimetry (DSC) results at the endo direction of iSkin, NaCl-laden tough hydrogel (N), glycerol-laden tough hydrogel (G), and original tough hydrogel in the temperature range from $-120\text{ }^{\circ}\text{C}$ to $15\text{ }^{\circ}\text{C}$. The small gray arrows highlight the melting points of the NaCl-laden tough hydrogel and the original tough hydrogel.

transparency, mechanical flexibility, and stretchability (twisting, bending, stretching, and knotting) at extremely cold conditions ($-30\text{ }^{\circ}\text{C}$ for 24 h, Figure 3C and Movie S3, Supporting Information) due to the large amount of unfrozen bound water. In contrast, the original tough hydrogels turned into an ice-like solid and was fragile when bending at $-30\text{ }^{\circ}\text{C}$ (Figure S6A and Movie S3, Supporting Information) owing to their large amount of “free water” stored in the hydrogel. The iSkin remained unfrozen even at $-70\text{ }^{\circ}\text{C}$ for at least 1 h (Figure S6B, Supporting Information). In addition, the iSkin also remained high conductivity under extremely cold environment ($5.34 \times 10^{-2}\text{ S m}^{-1}$ at $-25\text{ }^{\circ}\text{C}$ and $8.7 \times 10^{-3}\text{ S m}^{-1}$ at $-40\text{ }^{\circ}\text{C}$), which was superior to the original hydrogel (Figure 3D). The conductivity of the iSkin was maintained even at $-70\text{ }^{\circ}\text{C}$ ($1.96 \times 10^{-5}\text{ S m}^{-1}$), while the conductivity of the original hydrogel decreased to an unmeasurable level once below $-25\text{ }^{\circ}\text{C}$ (Figure 3D).

Besides the expected contribution from glycerol, the excellent anti-freezing property of the iSkin may also partially stem from the ice-inhibiting effect of the hydrogel networks^[33] and the electrolyte salts.^[49] To accurately determine the origin of the

antifreezing characteristic as well as the anti-freezing limits of the iSkin, we used differential scanning calorimetry (DSC) to test differently treated hydrogels and their exchanged solvents from $-120\text{ }^{\circ}\text{C}$ to $15\text{ }^{\circ}\text{C}$. During heating, the original (water-based) hydrogel began to melt from $-6.5\text{ }^{\circ}\text{C}$ and revealed a sharp melting peak occurred at $-1\text{ }^{\circ}\text{C}$ (labeled on the yellow curve in Figure 3E), which is consistent with the results from a previous report.^[49] The DSC testing result of the original hydrogel also shows a peak shift compared to that of the pure water (yellow curve at Figure S7A, Supporting Information). This slight peak shift can be attributed to the ice-inhibiting effect of Alg-PAAm polymer networks. We also found that pure electrolyte salt (NaCl) has a further ice-inhibiting effect on hydrogel as the melting point shifts from $-6.5\text{ }^{\circ}\text{C}$ to $-24\text{ }^{\circ}\text{C}$ (labeled on the green curve in Figure 3E). The melting point of NaCl-laden tough hydrogel shifts more than that of pure saturated NaCl solution at 5.4M ($-22\text{ }^{\circ}\text{C}$, labeled on the green curve in Figure S7A, Supporting Information), further confirming the ice-inhibiting effect of the Alg-PAAm networks. Notably, both the glycerol-laden hydrogel and the iSkin did not

show any melting peak in the entire endo/heating thermogram because these two types of hydrogel did not freeze and showed no cold-crystallization peak on the exo/cooling thermogram (Figure S8, Supporting Information), which is consistent with the previous reported observation.^[33] During heating, the glycerol-laden hydrogel and the iSkin only showed a peak similar to a glass transition at -97°C and -95°C , respectively (zoomed-in insets of blue and red curves in Figure 3E), indicating no observable icing of the hydrogels. This anti-freezing performance is better than most of the previously reported ionic hydrogels (Table 1).

In addition, we found that the presence of other components (e.g., NaCl and Alg-PAAm polymer networks) increased the glass transition point of glycerol-water system (66.6 wt%) to a higher temperature (blue and red curves in Figure 3E and red curve in Figure S7A, Supporting Information), which is due to the components' disturbance to the strong supercooling phenomenon in the glycerol-water system. In fact, the antifreezing and supercooling properties of the glycerol and the glycerol-laden hydrogel mainly depend on the glycerol-water ratio, as shown in Figure S7 (Supporting Information) (blue lines) and Figure S9 (Supporting Information); a lower glycerol concentration (e.g., 30 wt%, Figure S9A, Supporting Information) showed both crystallization and melting peaks on the DSC thermogram while higher ones (e.g., 66.6 wt%, blue curve in Figure S7, Supporting Information; and 85 wt%, Figure S9B, Supporting Information) have neither of peaks due to the strong supercooling effect. As a result, the freezing tolerance of tough hydrogel can be enhanced accordingly and such a simple solvent exchanging method is effective to enhance the freezing tolerance of hydrogels. These observations indicate that the iSkin could serve as a good anti-freezing stretchable sensing component for use on wearables and soft robots in extremely cold environments.

2.4. Surface Adhesion Testing of the iSkin

The strong adhesion of hydrogel to surfaces is a favorable feature for applications in wearable sensing and soft robotics. For on-skin wearable sensing, the iSkin should adhere tightly to the human skin to enhance the fidelity of signal acquisition and eliminate motion-induced signal artifacts. The self-adhesion of our pristine iSkin (Figure S10, Supporting Information) is not strong enough to withstand a heavyweight and rigorous deformation. In order to satisfy the adhesion requirement of various applications (e.g., smart clothes for underwater and/or extremely cold environments, wearables for sweaty and dynamically deformed human skin during sports, and smart wound dressing for wet organ surfaces during recovery monitoring), the iSkin should adhere to various surfaces firmly during wearing. The adhesion property of the iSkin for different substrates with different surface conditions was investigated. The adhesion energy was quantified by T-peeling tests (setup shown in Figure S11, Supporting Information).

First, we chose porcine skin ($L \times W$: 80 mm \times 15 mm) as the model for iSkin-skin bonding testing as porcine skin closely resembles the surface property of human skin. The porcine skin is mechanically robust and tough enough to prevent cracks

or fractures on the skin itself during the T-peeling test, thus making the ultimate adhesion failure to be cohesive failure that always occurs at the iSkin-porcine skin interface. Due to the bridge polymer interpenetration and the covalent bonding between amino and carboxyl groups on skin and hydrogel surfaces, the adhesion energy of the iSkin to the regular porcine skin was 5374 J m^{-2} (pink curve in Figure 4A,B, Movie S4, Supporting Information), which indicates strong adhesion.^[29] External ions may hamper the adhesion capability by disturbing the positively charged primary amine groups of bridge polymer and thus the formation of both imine and ionic bonds.^[50] However, we found that the interfacial adhesion energy of the iSkin-skin bonding has no significant difference with that of hydrogel-skin bilayer bonded with the same bridge polymer layer (Figure S12, Supporting Information), proving that the presence of neutrally charged glycerol can suppress the side effect of pure ions to the adhesion performance.

In addition, most ionic hydrogel devices do not have strong adhesion capability to wet surfaces (Table 1). The adhesion formation of a hydrogel device with natural skin is often complicated because of the sweating and dynamic movements of the skin. Sweating is inevitable in real life especially during long-term wearable sensing (e.g., during sport and exercise). To simulate the sweating condition on natural skin, the porcine skin was first covered with artificial sweat (Figure S13B, Supporting Information) before the attachment of an iSkin. The adhesion energy of sweaty iSkin-skin bonding was found to be 649.3 J m^{-2} (black curve in Figure 4A,B,D, Movie S4, Supporting Information), which shows a slightly higher adhesion performance than that (5374 J m^{-2}) without sweat exposure, confirming strong wet adhesion capability. Similarly, we chose nylon fabric (the out-layer of most winter coats such as Canada Goose) as the model substrate to mimic the adhesion between the iSkin and the winter coat. We found that the iSkin can adhere strongly to the carboxylated nylon fabric with an adhesion energy 398.4 J m^{-2} (red curve in Figure 4A,B, Movie S4, Supporting Information), while the bonding between iSkin and the pristine nylon fabric is weak (79.7 J m^{-2}) due to the non-existence of carboxyl groups. This strong bonding is mainly because primary amine groups within the bridging polymer covalently bind with the carboxyl groups from the carboxylated nylon fabric and the iSkin matrix.

Furthermore, we studied its anti-freezing and long-term adhesion capability to different substrates. As shown in Figure 4C, the adhesion between the iSkin and substrates (adhesion area: $1.3 \times 5.5 \text{ cm}^2$) securely held a 1 kg weight (14.0 kPa) in both dried and humid environments for more than 30 d (Figure 4E,F). In addition, the adhesion between the iSkin and nylon fabric at underwater or subzero temperature environment was comparable to that of the original one; that is, the iSkin-nylon fabric adhesion held a 500 g weight (7.0 kPa) at the underwater environment for more than 20 h (Figure S13A, Movie S5, Supporting Information) and held a 1 kg weight (14.0 kPa) at -30°C for more than 24 h (Figure 4G, Movie S5, Supporting Information). The adhesion maintenance of the iSkin at low temperature could be attributed to the diffusion of glycerol into the thin adhesion layer and the inhibition of ice formation in this layer. This strong surface adhesion under diverse conditions ensures the fidelity of signal acquisition

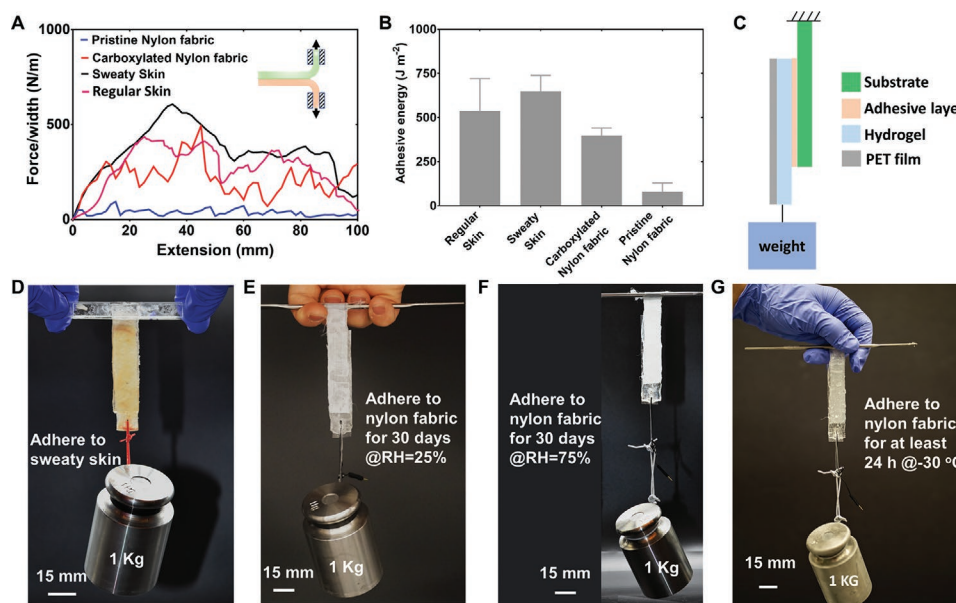


Figure 4. Surface adhesion property of the iSkin. A) Force/width curve for adhesion between the iSkin and different substrate surfaces. B) Comparison of the adhesive energy between different substrate surfaces. C) Schematic setup of the adhesion test between the iSkin and diverse substrate surfaces. D) The adhesion stability of iSkin adhered to sweaty porcine skin. E) The long-term adhesion capability of iSkin adhered to carboxylated nylon fabric at the relatively dry environment (RH = 25%). F) The long-term adhesion capability of iSkin adhered to carboxylated nylon fabric at relatively wet environment (RH = 75%). G) The anti-freezing adhesion capability of iSkin adhered to carboxylated nylon fabric. Subzero temperature is -30°C .

from the iSkin device as a sensing component on wearables and soft robots in diverse environments.

To our best knowledge, this is the first reported conductive ionic hydrogel with high stretchability, high toughness, long-term stability, superior diverse adhesion capability, and anti-freezing behavior, making it particularly useful for the construction of adhesive ionic skins for applications in various extreme environments. Note that both ion-related mechanical and adhesive properties were either enhanced or maintained due to the presence of glycerol, despite the disturbance from monoions.

2.5. Adhesive iSkin for Wearable Sensing and Human–Machine Interaction

Thanks to the unique combination of mechanical, electrical, anti-freezing, and surface adhesion properties, our iSkin can serve as wearable strain sensors for joint gait measurement and human–machine interaction. Here, an iSkin strain sensor of $80 \times 25 \times 1.4 \text{ mm}^3$ was attached to the elbow joint position of a winter coat. The iSkin can firmly adhere to the winter coat surface during arm bending at subzero temperature (-10.6°C in Figure 5A and Figure S14, Supporting Information). Due to its good conductivity, high stretchability, and freezing-tolerant adhesion capability at low temperature, the iSkin strain sensor can monitor the bending-release motions of an arm at -10.6°C without debonding from the winter coat (Figure 5B). This capability can be utilized to design smart winter clothes with iSkin strain sensors for extreme environment applications.

We also demonstrated on-skin strain sensing during user exercise. In this application, the iSkin should always adhere

strongly to the human skin whether the skin is dry, wet (e.g., with sweat), and/or in dynamic movement conditions. By applying a thin layer of adhesive bridge polymer, a piece of iSkin ($80 \times 25 \times 1.4 \text{ mm}^3$) was attached to the knee of a volunteer for gait measurement (Figure 5C). Compared with the pristine iSkin, the adhesive iSkin can firmly adhere to the knee after multiple vigorous jumps (Figure S15, Movie S6, Supporting Information). Furthermore, we found that this strong adhesion can endure a long-term vigorous workout (e.g., 30 min step-up) without debonding from the sweaty and dynamically stretched skin surface (Figure 5C, Figure S16C,D, Movie S6, Supporting Information). As expected, our iSkin has no observable adverse effect on the skin once detached (Figure S16A ,B, Supporting Information), thanks to the excellent biocompatibility of the iSkin material system. In addition, the resistance output of the iSkin for walking gait measurement is highly repeatable before and after this 30-min vigorous workout (Figure 5D), further proving the strong and robust on-skin adhesion and reliable strain sensing capability of the iSkin.

The wearable iSkin strain sensor can also be used for constructing a gesture-based interface for human-machine interaction. We constructed a strain-sensing glove by attaching a piece of iSkin ($30 \times 10 \times 1.4 \text{ mm}^3$) on each finger (Figure 5E) of a surface-functionalized Ecoflex glove (glove fabrication and preparation described in the Experimental section). The resistance of each iSkin piece changed proportionally with the bending angle of its corresponding finger joint (Figure 5I). The resistance change was converted into a voltage change through a voltage divider circuit and read by an Arduino UNO board. Due to the strong bonding between Ecoflex and iSkin (to be further discussed in the next section), a user wearing the glove

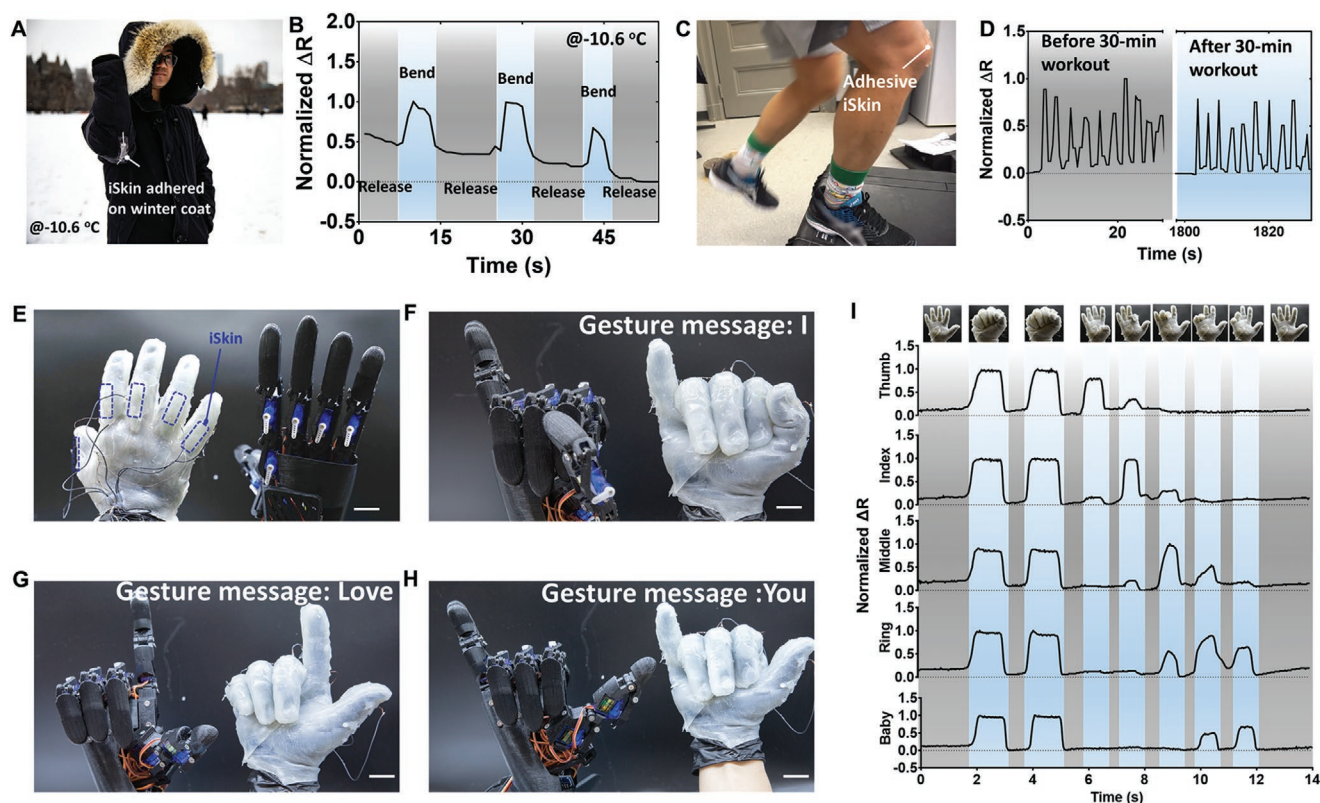


Figure 5. Adhesive iSkin for wearable demonstrations and human–machine interaction. A) Anti-freezing iSkin adhered to a winter coat for strain sensing at -10.6°C . B) Repeatable normalized resistance change (ΔR) of the wearable iSkin on the winter coat for arm motion monitoring at -10.6°C . C) Schematic setup of iSkin adhered to the knee for gait measurement, showing good adhesion capability when adhered to a dynamic and sweaty skin surface during long-term vigorous workout (e.g., step-up). D) Normalized ΔR of iSkin adhered to the knee for walking gait measurement. E) Schematic setup of iSkin (denoted within purple dash rectangle) adhered homemade glove (00-35 Ecoflex) for human–machine interaction. F–H) Demonstrations of the robotic hand controlled by human hand gestures to show “I,” “Love,” “You.” Scale bar: 2 cm. I) Normalized ΔR of iSkin is plotted as a function of time during a sequence of finger gestures, in which the iSkins were adhered on each finger joint of the glove.

can reliably control the gesture of a robotic hand due to the high signal fidelity of the iSkin strain sensors (Movie S7, Supporting Information). As a demonstration, the robotic hand was controlled by the glove to express the message of “I love you” with three sequential hand gestures (Figure 5F–H and Movie S7, Supporting Information). This demonstration highlights the feasibility of using our iSkin for human–machine interaction.

2.6. Adhesive iSkin for Strain Sensing on Soft Grippers and Locomotive Soft Robots

The large-strain sensing capability of the highly stretchable iSkin would also be highly useful for strain sensing on soft robots. Recently, soft robotic systems have been developed to bridge the gap between machines and people due to their unprecedented adaptability.^[51] Constructed from intrinsically soft and/or stretchable materials, soft robots hold great potential for many applications, including manipulation of fragile objects, navigation in space-restricted and/or harsh environments, and human rehabilitation and assistance. For strain/deformation measurement on soft robots, it is highly desired to develop stretchable strain sensors that are made from materials compatible with soft robot materials and can be readily integrated into

existing soft robot designs.^[11,12,51] With comparable mechanical properties to Ecoflex and other commonly used elastomers in soft robots, our iSkin is mechanically compatible with typical soft robot designs. The strong surface adhesion capability of the iSkin on elastomers will also enable the flexible integration of strain sensors during or after soft robot fabrication. In this section, we demonstrate the facile integration of iSkin strain sensors onto two typical soft robotic systems—a soft gripper and a quadruped soft robot—to endow them with reliable deformation feedback under both normal and extreme conditions. Importantly, different from other hydrogel-based ionic sensors,^[12,43] the unique combination of high ambient stability, excellent anti-freezing property, and strong adhesion capability (for diverse material surfaces) of the iSkin could further expand the scope of its applications in soft robotics.

We first demonstrated the strong bonding between iSkin and Ecoflex through a bonded bilayer of 1.4 mm thick iSkin and 100 μm thick Ecoflex (Ecoflex 00-50, Smooth-On Inc.). Instead of using the bridge polymer adhesive layer, here the iSkin was bonded to the Ecoflex using an alternative strategy that has revealed the largest hydrogel–elastomer adhesion energy reported ever.^[52,53] This strong iSkin–Ecoflex adhesion stems from in situ chemical grafting of methacrylate groups on the surface of the chemisorbed Ecoflex to the PAAm network

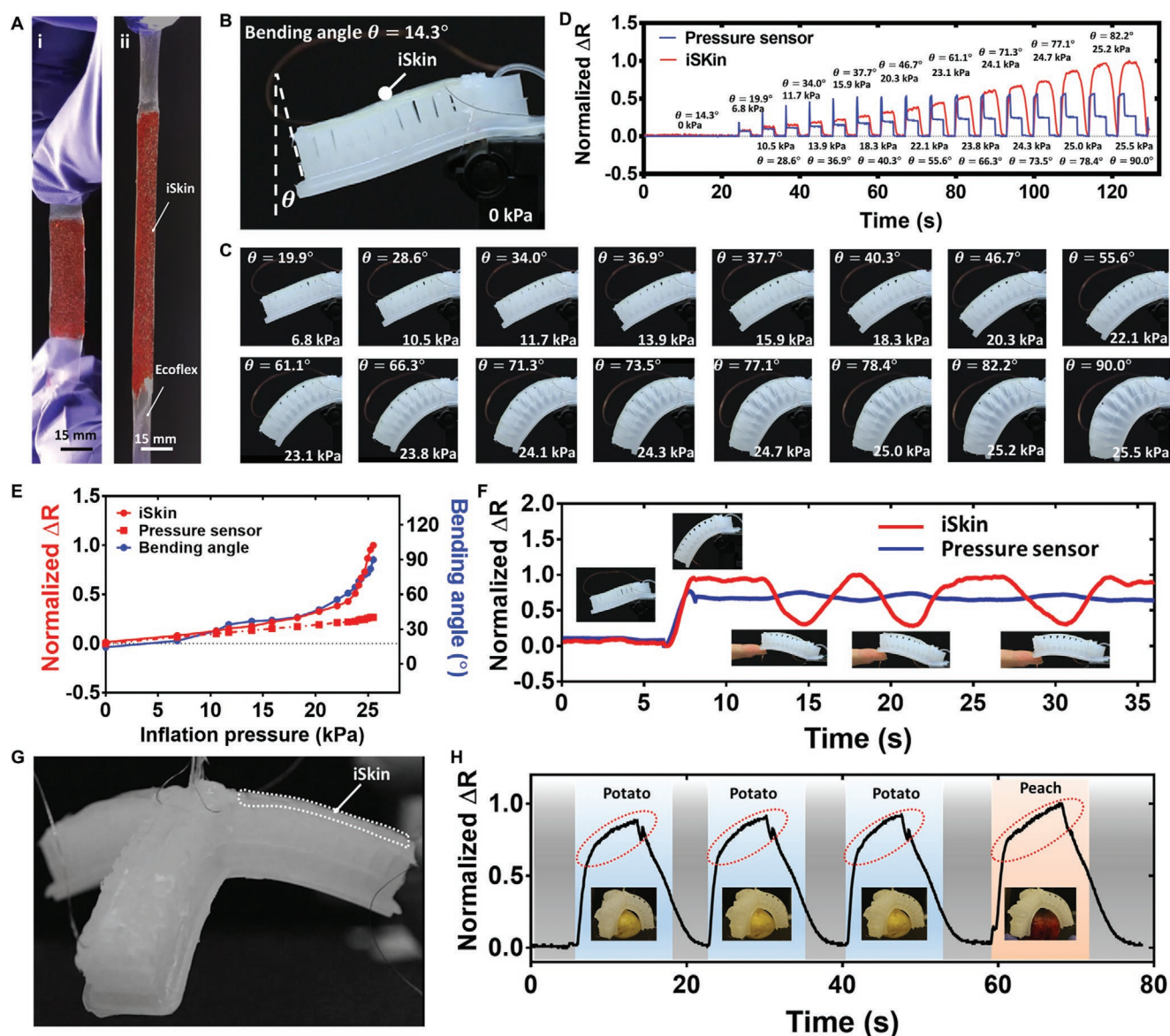


Figure 6. Performance of iSkin-equipped smart soft actuators. A) The strong adhesion between iSkin and Ecoflex can endure large stretch (at least 150%). Note that red food dyes are stained on iSkin to enhance the contrast between iSkin and elastomers. Images of an iSkin-equipped smart soft actuator at B) 0 kPa and C) during a dynamic free displacement test, in which the actuator experiences periods of deflation (0 kPa) to increasing inflation pressure (held for 2.5 s) in increments of 6.8–25.5 kPa. D) iSkins endow soft actuators with the ability to sense their actuated state. Resistance change (ΔR) of iSkin and a commercial inflation pressure sensor are plotted as a function of time during inflation. E) Normalized ΔR for iSkin and the commercial inflation pressure sensor, and bending angle θ , as a function of inflation pressure read from a pressure meter during free displacement. F) Normalized ΔR for iSkin and the commercial inflation pressure sensor is plotted as a function of time when an iSkin-equipped smart soft actuator was undergoing three times hand bending, in which the actuator is in inflation status. Inset figures show the soft actuators under a different status. G) Optical photo of an iSkin-equipped smart soft robotic gripper. H) Normalized ΔR of an iSkin is plotted as a function of time during fruits and vegetable grabbing. The curve shape difference within the red dash circle during the grabbing procedure can differentiate various kinds of fruits and vegetables. Inset figures show the soft robotic gripper grabbing a potato and a peach.

during curing.^[52] Nevertheless, the bridge polymer adhesive layer we demonstrated in previous sections is still effective to create strong bonding between iSkin and Ecoflex or other elastomers through surface functionalization of the elastomer surface with amine^[54] and/or carboxyl^[50] groups. The strong hydrogel–Ecoflex bonding was maintained after adding anti-freezing and electrolyte compounds into the hydrogel matrix of the iSkin, and this adhesion can endure large stretching

[>150%, beyond the strain limit (100%–150%) of most soft robots^[39]] without debonding (Figure 6A, Movie S8, Supporting Information).

We then characterized the performance of an iSkin-equipped soft bending actuator (Figure 6B). A piece of iSkin ($50 \times 18 \times 1.4 \text{ mm}^3$) was attached to the top surface of the bending actuator for bending angle measurement. Cyclic inflation–deflation testing was conducted, during which the actuator

was repeatedly inflated (with a constant pressure for 2.5 s) and deflated (with zero input pressure for 2.5 s) with the inflation pressure increasing cycle by cycle from 6.8 to 25.5 kPa (Figure 6C and Movie S9, Supporting Information). The iSkin firmly adhered to the actuator surface during repeated bending of an bending angle θ ranging from 0° to 90°, and no debonding occurred during the entire test (Figure 6C and Movie S9, Supporting Information). The attachment of the iSkin layer with mechanical properties comparable to Ecoflex had no obvious impact on the operation of the actuator (Movie S9, Supporting Information). The resistance change ΔR of the iSkin (Figure 6D,E) increased with the actuator bending angle θ faithfully and in real time during the entire inflation-deflation period. In contrast, the inner pressure of the actuator, monitored by a pressure sensor, only dramatically increased at the beginning of the inflation period then rapidly dropped and stabilized at a much lower level (blue curve in Figure 6D) because of the air leakage through Ecoflex; both the initial peak value or the stabilized value of the actuator inner pressure did not correlate with the actuator bending angle. This result proves that the iSkin can provide more reliable deformation/position feedback for a soft actuator than its inner pressure. In addition, we repeatedly exerted an upward force to the free end of the inflated bending actuator with an initial angle of 60° (insets in Figure 6F and Movie S10, Supporting Information), and found that the iSkin resistance decreased upon force application and always recovered to its initial value after force removal (red curve in Figure 6F, and Movie S10, Supporting Information), while the actuator inner pressure did not change noticeably with the force applied and removed (blue line in Figure 6F and Movie S10, Supporting Information). This observation further illustrates that the iSkin integrated into a soft robotic system could provide human-like sensing feedback indicating robot-environment interaction. The adhesion-enabled integration of pre-fabricated iSkin sensors onto soft robots provides a general and facile strategy for developing position- and force-feedback soft robots.

To further demonstrate the utility of iSkin sensing feedback, we integrated three iSkin sensors ($50 \times 18 \times 1.4 \text{ mm}^3$) on a soft gripper for object grasping (Figure 6G). The soft gripper was inflated continuously to grasp an object (potato or peach in our experiments) until a secured grabbing was achieved and then deflated to its natural initial shape, during which the resistance values of the three iSkin sensors were continuously monitored. It was found that the slope of the measured resistance curve decreases obviously upon contact between the gripper arm and the object (Figure 6H and Movie S11, Supporting Information). Resistance curves of the same iSkin sensor from the repeated grasping of the same potato are highly consistent, which proves the high repeatability and robustness of the iSkin sensor. No obvious difference was observed in the resistance curves of the three iSkin sensors during the same grasping process. The slope-changing portion of the resistance curve measured during object grasping (labeled with dashed ovals in Figure 6H) could be potentially utilized, together with other feedback modalities (e.g., contact forces and curvature distributions of the gripper arms), for shape classification and object recognition during grasping, through learning-based algorithms.^[11,55] Equipped with the anti-freezing iSkin sensors, such a soft gripper could be used for robotic manipulation tasks in extremely cold

environments (e.g., pick and place of frozen food items in cold storage rooms).

Most of the previous studies focused on developing sensing technologies for soft robots in the normal temperature range,^[12,16,43,51,56,57] there is little research on the performance of soft robotic sensors under extremely cold conditions. In addition, strong adhesion between hydrogel-based ionic sensors and soft robots under the subzero temperature has not been reported. Here we first studied the bonding between iSkin and soft robots under the subzero environment. The bonded iSkin–Ecoflex bilayer presented in Figure 6A was stored at -30°C for overnight before testing. The strong adhesion between the iSkin and Ecoflex was maintained well in such cold temperature, and the anti-freezing adhesion can still endure large stretching ($>110\%$) without any debonding (Figure S17A, Movie S12, Supporting Information). This meets the requirement of soft/stretchable sensors for many soft robotic applications in an extremely cold environment. In contrast, a bonded bilayer of the original tough hydrogel and Ecoflex layer cannot be stretched anymore after overnight storage at -30°C , due to the freezing of the original hydrogel (Figure S17B, Movie S12, Supporting Information).

Then, we integrated iSkin sensors (colored by red dye) onto a classical quadruped soft robot to provide motion feedback of the five pneumatic actuators on the robot (Figure 7A). Four U-shaped iSkin sensors were individually adhered onto four legs of the robot, and one S-shaped iSkin sensor on the middle body part. Because of its excellent anti-freezing property, the iSkin is still highly stretchable at subzero temperature and thus does not add obvious restriction to the compliance of the soft robot. Figure 7B shows the locomotion sequence of the soft robot operating on outdoor snow at -5.3°C (Movie S13, Supporting Information), during which the five iSkin sensors strongly adhered to the robot body and provided reliable motion feedback signals. This excellent adhesion and anti-freezing performance is essential for developing a motion-feedback soft robot operating in extremely cold conditions. Movie S13 (Supporting Information) presents the two locomotion modes (walking and crawling) of the iSkin-equipped quadruped soft robot on the snow. One can see that the iSkin has little compliance restriction on the locomotion of the soft robot at low temperature due to the unique shape design and the mechanical stretchability of iSkin in such a harsh environment. Under walking mode, current pressurizing patterns can produce forward locomotion at a speed of 0.56 m h^{-1} (4 body lengths h^{-1}) on the snow (Figure S18, Movie S13, Supporting Information).

To further test the robot in a colder environment, we operate the robot in a freezer chamber (-22°C , Figure S19A, Supporting Information) and measured the feedback signals from the five iSkin sensors. During the entire testing of 500 locomotion cycles of the robot, there was no debonding of the iSkin observed (Movies S14 and S15, Supporting Information), confirming the feasibility of long-term use of the iSkin at freezing temperature. At -22°C , the robot can produce forward walking locomotion at a speed of 1.2 m h^{-1} (8.5 body lengths h^{-1} , Figure S19, Movie S14, Supporting Information) and forward crawling locomotion at a speed of 1 m h^{-1} (7 body lengths h^{-1} , Figure S20, Movie S15, Supporting Information). During the test, the iSkin sensors provided real-time motion feedback of the locomotive gaits of the five pneumatic actuators (walking

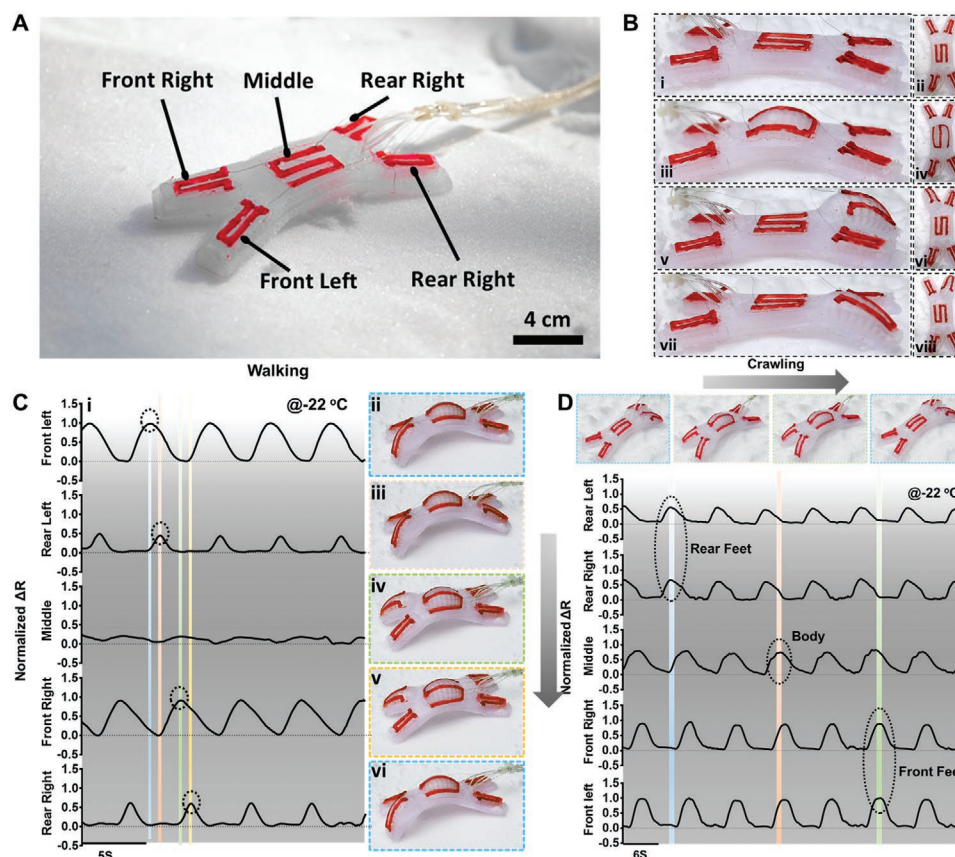


Figure 7. Performance of iSkin-equipped intelligent soft robots at the subzero environment. A) An optical photographs of an iSkin-equipped pneumatic soft robot. The U-shape iSkins were bonded on the front right, front left, rear right, and rear left feet/ pneumatic chamber, and Z-shape iSkin bonded on the body (middle). Note that red food dyes are stained on iSkin to enhance the contrast between iSkin and elastomers. B) Optical photographs of an iSkin-equipped pneumatic soft robot under different inflation stages: (i, iii, v, vii) side view and (ii, iv, vi, viii) top view of the robot under depressurization, body (middle), left and right foot under inflation sequentially. There is no debonding occurring between iSkin and Ecoflex robot during cyclic inflation-deflation from the side view figures. C) iSkins endow soft robot with the ability to sense their actuated state and gait patterns even at an extremely cold environment. Normalized ΔR of five iSkins is plotted as a function of time when soft robot is under walking gait at $-22\text{ }^{\circ}\text{C}$ (i) and optical photos of the soft robot during a sequence of dynamic walking on the snow (ii–vi). D) Optical photographs of the soft robot during a sequence of dynamic crawling on the snow (i–iv) and normalized ΔR of five iSkins is plotted as a function of time when the soft robot is under crawling gait at $-22\text{ }^{\circ}\text{C}$ (v).

gait feedback shown in Figure 7C and Movie S14, Supporting Information; crawling gait feedback shown in Figure 7D and Movie S15, Supporting Information). These results show that the iSkin strain sensor possesses high material compatibility, easy-to-attach surface adhesion capability, and excellent anti-freezing property suitable for sensing applications on soft robots operating in extremely cold environments.

2.7. Conclusions and Discussion

In this study, we reported the design, fabrication, and characterization of a novel adhesive hydrogel-based ionic skin (iSkin), and demonstrated its applications in wearable sensing and soft robotics. The iSkin recapitulates the salient features of human skin by combining high toughness and stretchability, ambient stability, anti-freezing property, and strain sensing capability. Our results demonstrated that the iSkin has a toughness of 11.41 kJ m^{-2} and can sustain more than 1975% strain without rupture, which is mainly attributed to the hybrid cross-linked

network design of the material, namely the synergistic effect of ionic cross-linked alginate and covalently cross-linked PAAm networks. Importantly, we discovered that the combination of glycerol and concentrated salts overcomes the issue of reduced toughness and stretchability of alginate-PAAM hydrogel caused by the incorporation of monovalent ions (e.g., K^+ , Na^+ , and Cl^-) that unzip the calcium-alginate ionic bonds. In addition, due to the unique chemical structure of tough hydrogel and negligible electrical effect of neutral hygroscopic/cryoprotective substance, the positively charged bridge polymer within the adhesive layer of the iSkin can penetrate into both the tough hydrogel and the target surface (e.g., natural skin), forming strong adhesion by electrostatic interactions, physical entanglement, and chemical anchoring. We revealed that the incorporation of glycerol prevents the reduction of interfacial adhesion energy of the EDC/NHS coupling layer (due to the external disturbances such as the concentrated salts^[58]). The iSkin showed both strong dry and wet adhesion capability to different substrate surfaces including natural skin and cloth fabric with the adhesion energy of 398 and 649 J m^{-2} , respectively.

Moreover, the inclusion of the neutral hygroscopic substance glycerol and the electrolyte NaCl maintains the electrical conductivity of the iSkin, and substantially improves the stability of its conductivity, physical and adhesive properties both in ambient and extremely cold environments. The iSkin has an ambient conductivity of 0.904 S m^{-1} (comparable to that of other similar conductive ionic hydrogels) and can maintain its electrical property after 1300 cycles of stretching and one month storage in the ambient environment. With an extremely low temperature tolerance (-95°C), the iSkin show measurable conductivity of $1.96 \times 10^{-5} \text{ S m}^{-1}$ even at -70°C . In addition, the strong iSkin–substrate bonding showed long-term stability both in dry/wet environments and at extremely low temperatures (at least -30°C). Thanks to the unique combination of mechanical, physical, and electrical properties, the iSkin can find numerous applications such as smart winter coat with strain sensing capability, wearable exosuit for gait measurement, stretchable electronic glove for human–machine interaction, motion-feedback soft robots operating in cold environments.

While this work was focused on the design, characterization, and proof-of-concept demonstration of the iSkin, further research is needed to increase the integration level and improve the performance of the iSkin. For instance, microfabrication and 3D printing methods need to be developed for constructing micrometer-sized iSkin components and realizing more complex designs such as microsensor arrays for enhanced spatial sensing resolution.^[47,59,60] In addition, similar to other types of stretchable hydrogel sensor, the repertoire of ionic devices could be expanded to achieve other functionalities, for instance, sensing of humidity,^[60] temperature, pH,^[61] glucose,^[62] and other biomolecules and chemicals.^[17] Such multimodal sensing capabilities of the iSkin can potentially empower wearables and soft robots with a higher level of intelligence for more sophisticated tasks. Moreover, the iSkin is potentially an excellent conductive material to fabricate ultrastretchable triboelectric nanogenerator, which can serve as stretchable and portable power sources for seamless integration with untethered wearables and soft robots.^[51,63] Last but not least, the adhesion method based on the bridging polymer adhesive needs to be further improved to shorten the relative long time to form strong adhesion (5–30 min),^[29,53] which may be solved by the recent developed dry double-sided adhesive tape working for a variety of material surfaces.^[54]

In summary, we developed the highly stretchable, anti-freezing, ambient-stable iSkin inspired by the salient features of human skin. With strong surface adhesion capability, the iSkin is highly suitable for wearable sensing and soft robotics. The presented design and fabrication approach to construct mechanically and electrically robust hydrogel is also applicable to constructing other hydrogel-based material systems. We envision that the results presented here will lead to the development of next-generation wearable devices and soft robotic systems with human-like sensation.

3. Experimental Section

Materials: Ionic cross-linker calcium sulfate (CaSO_4 , 255548), Alginate (A2033), acrylamide (AAm, A8887), covalent cross-linker N,N'-methylenebis(acrylamide) (MBAA, M7279), free-radical initiator ammonium persulfate (APS, A3678), polymerization accelerator tetramethyl-ethylenediamine (TEMED, T7024), photoinitiator IRGACURE

2959 (I2959), acetic acid (695092), sodium chloride, bridging polymer chitosan of medium molecular (448877), the coupling reagents, 1-ethyl-3-(3-dimethylaminopropyl) carbodiimide hydrochloride (EDC, E1769) and n-hydroxysulfosuccinimide (sulfo-NHS, 56485), hygroscopic substance glycerol (G9012), and humidity control reagent lithium chloride (LiCl , 793620) were purchased from Sigma. Hydrochloric acid (HCl , 9H61734) was purchased from Bioshop. Artificial sweat with PH 5.5 was purchased from Taobao. Milli-Q ($18.3 \text{ M}\Omega$) water was used in all experiments. Porcine skin was purchased from a local grocery store. Pure nylon fabric was purchased from Amazon.

Fabrication of the iSkin: The fabrication process consists of three steps: i) the synthesis of dissipative matrix alginate-polyacrylamide (Alg-PAAm) tough hydrogel; ii) solvent exchange; and iii) adhesive layer coating. The detailed protocol can be found in Supporting Information.

Fabrication of Strain-Sensing Glove, Soft Gripper, and Quadraped Soft Robot: The smart glove for human–machine interaction was fabricated as followed: The precured Ecoflex A and B (00-35 fast, Smooth-On Inc.) were mixed quickly and our human-like model hand was dipped into the mixture entirely and then cured in the open air for 5 min. Flesh bonded elastomer-iSkin was then adhered to the finger joint of the glove with coating a thin layer of precured Ecoflex as glue. Metal wires were used for connecting iSkin to control a robotic hand to make gestures accordingly. Robotic hand (Youbionic Robot Right Hand 2019) was purchased on RobotShop. The fabrication of soft robots and grippers has been reported previously,^[14,64,65] and here we will only introduce the adhesion process of the iSkin to the soft gripper and robot. Similarly, flesh bonded Ecoflex-iSkin was adhered to the soft gripper and robot with coating a thin layer of pre-cured Ecoflex on the Ecoflex side as glue. Once cured, the metal wires were used for connecting the iSkin to Arduino boards for electrical data acquisition and gait pattern control.

Statistical Analysis: Statistical analyses were performed on GraphPad Prism software (GraphPad Software, Inc.). Results are depicted as mean \pm standard deviation (SD), and unpaired Student's *t* test was conducted to analyze the statistical differences of experiment results. Parametric test was used by assuming any experimental groups are normally distributed with the same SD. Differences were considered statistically significant if $P < 0.05$.

Testing of the iSkin on Human Knees: The tests of the devices on human body described here do not need Institutional Review Board (IRB) approval, because the experiments do not affect living people physically or physiologically and one has not sought or received identifiable private information. The hand and knees shown in the Table of Contents image and Figures 5, 6, S10, S15, and S16 are those of B.Y., who has given his consent to publish these images. Informed signed consent was obtained from B.Y. for their participation in the experiments.

Supporting Information

Supporting Information is available from the Wiley Online Library or from the author.

Acknowledgements

This work was supported by the Natural Sciences and Engineering Research Council of Canada (RGPIN-2017-06374, RGPAS 2017-507980, and RGPIN-2018-04146), the Canada Foundation for Innovation (JELF-37812 and JELF-37719), and the University of Toronto. The authors acknowledge Prof. Mitchell Winnik and Prof. Yu Zou for the access to a tensile tester and a DSC, and Dr. Yang Liu, Dr. Hang Zhou and Prof. Mitchell Winnik for the technical assistance on the usage of the DSC. The authors also thank the technical advice about bioadhesives from Guangyu Bao and Zhenwei Ma.

Conflict of Interest

The authors declare no conflict of interest.

Author Contributions

R.Z.C. and R.Z. contributed equally to this work. B.Y., J.L.L., and X.L. conceived the idea and designed experiments. B.Y. and R.Z.C. carried out material preparation and characterization. B.Y., R.Z.C., and R.Z. carried out the experiments of strain sensing, human-machine interaction, and soft robotics. B.Y., R.Z.C., R.Z., and X.L. performed data analysis. B.Y. and X.L. wrote the manuscript with input from all the other authors. All authors contributed to and agree with the content of the final version of the manuscript.

Data Availability Statement

The data that support the findings of this study are available from the corresponding author upon reasonable request.

Keywords

anti-freezing hydrogel, diverse surface adhesion, human-machine interface, ionic skin, soft robotics, stretchable electronics

Received: May 17, 2021
Published online: July 28, 2021

- [1] W. Yang, V. R. Sherman, B. Gludovatz, E. Schaible, P. Stewart, R. O. Ritchie, M. A. Meyers, *Nat. Commun.* **2015**, 6, 6649.
- [2] K. Laden, R. Spitzer, *J. Soc. Cosmet. Chem.* **1967**, 18, 351.
- [3] Y. Lee, C.-H. Lee, U. Oh, *Mol. Cells* **2005**, 20, 315.
- [4] Y. Roudaut, A. Lonigro, B. Coste, J. Hao, P. Delmas, M. Crest, *Channels* **2012**, 6, 234.
- [5] A. Chortos, J. Liu, Z. Bao, *Nat. Mater.* **2016**, 15, 937.
- [6] Y. Sun, W. M. Choi, H. Jiang, Y. Y. Huang, J. A. Rogers, *Nat. Nanotechnol.* **2006**, 1, 201.
- [7] D.-H. Kim, N. Lu, R. Ghaffari, Y.-S. Kim, S. P. Lee, L. Xu, J. Wu, R.-H. Kim, J. Song, Z. Liu, *Nat. Mater.* **2011**, 10, 316.
- [8] J. Y. Sun, C. Keplinger, G. M. Whitesides, Z. Suo, *Adv. Mater.* **2014**, 26, 7608.
- [9] W. B. Ying, Z. Yu, D. H. Kim, K. J. Lee, H. Hu, Y. Liu, Z. Kong, K. Wang, J. Shang, R. Zhang, *ACS Appl. Mater. Interfaces* **2020**, 12, 11072.
- [10] B. Ying, Q. Wu, J. Li, X. Liu, *Mater. Horiz.* **2020**, 7, 477.
- [11] B. Shih, D. Shah, J. Li, T. G. Thuruthel, Y.-L. Park, F. Iida, Z. Bao, R. Kramer-Bottiglio, M. T. Tolley, *Sci. Rob.* **2020**, 5, eaaz9239.
- [12] C. Larson, B. Peele, S. Li, S. Robinson, M. Totaro, L. Beccai, B. Mazzolai, R. Shepherd, *Science* **2016**, 351, 1071.
- [13] J. W. Booth, D. Shah, J. C. Case, E. L. White, M. C. Yuen, O. Cyr-Choiniere, R. Kramer-Bottiglio, *Sci. Rob.* **2018**, 3, eaat1853.
- [14] S. Y. Kim, Y. Choo, R. A. Bilodeau, M. C. Yuen, G. Kaufman, D. S. Shah, C. O. Osuji, R. Kramer-Bottiglio, *Sci. Rob.* **2020**, 5, eaay3604.
- [15] T. G. Thuruthel, B. Shih, C. Laschi, M. T. Tolley, *Sci. Rob.* **2019**, 4, eaav1488.
- [16] H. Zhao, K. O'Brien, S. Li, R. F. Shepherd, *Sci. Rob.* **2016**, 1, eaai7529.
- [17] K. B. Justus, T. Hellebrekers, D. D. Lewis, A. Wood, C. Ingham, C. Majidi, P. R. LeDuc, C. Tan, *Sci. Rob.* **2019**, 4, eaax0765.
- [18] H. Sheng, X. Wang, N. Kong, W. Xi, H. Yang, X. Wu, K. Wu, C. Li, J. Hu, J. Tang, *Extreme Mech. Lett.* **2019**, 30, 100510.
- [19] H. R. Lee, C. C. Kim, J. Y. Sun, *Adv. Mater.* **2018**, 30, 1704403.
- [20] C. Yang, Z. Suo, *Nat. Rev. Mater.* **2018**, 3, 125.
- [21] M. Zhu, X. Wang, H. Tang, J. Wang, Q. Hao, L. Liu, Y. Li, K. Zhang, O. G. Schmidt, *Adv. Funct. Mater.* **2019**, 30, 201907218.
- [22] X. Liu, J. Liu, S. Lin, X. Zhao, *Mater. Today* **2020**, 36, 102.
- [23] Z. Lei, P. Wu, *Nat. Commun.* **2018**, 9, 1.
- [24] C.-C. Kim, H.-H. Lee, K. H. Oh, J.-Y. Sun, *Science* **2016**, 353, 682.
- [25] J. Ge, L. Sun, F. R. Zhang, Y. Zhang, L. A. Shi, H. Y. Zhao, H. W. Zhu, H. L. Jiang, S. H. Yu, *Adv. Mater.* **2016**, 28, 722.
- [26] H. Yuk, T. Zhang, S. Lin, G. A. Parada, X. Zhao, *Nat. Mater.* **2016**, 15, 190.
- [27] T. Yamada, Y. Hayamizu, Y. Yamamoto, Y. Yomogida, A. Izadi-Najafabadi, D. N. Futaba, K. Hata, *Nat. Nanotechnol.* **2011**, 6, 296.
- [28] J.-Y. Sun, X. Zhao, W. R. Illeperuma, O. Chaudhuri, K. H. Oh, D. J. Mooney, J. J. Vlassak, Z. Suo, *Nature* **2012**, 489, 133.
- [29] J. Li, A. Celiz, J. Yang, Q. Yang, I. Wamala, W. Whyte, B. Seo, N. Vasilyev, J. Vlassak, Z. Suo, *Science* **2017**, 357, 378.
- [30] T. Liu, M. Liu, S. Dou, J. Sun, Z. Cong, C. Jiang, C. Du, X. Pu, W. Hu, Z. L. Wang, *ACS Nano* **2018**, 12, 2818.
- [31] H. Liu, M. Li, C. Ouyang, T. J. Lu, F. Li, F. Xu, *Small* **2018**, 14, 1801711.
- [32] H. Liu, M. Li, S. Liu, P. Jia, X. Guo, S. Feng, T. J. Lu, H. Yang, F. Li, F. Xu, *Mater. Horiz.* **2020**, 7, 203.
- [33] F. Chen, D. Zhou, J. Wang, T. Li, X. Zhou, T. Gan, S. Handschuh-Wang, X. Zhou, *Angew. Chem., Int. Ed. Engl.* **2018**, 57, 6568.
- [34] W. P. Williams, P. J. Quinn, L. I. Tsonev, R. D. Koyanova, *Biochim. Biophys. Acta, Biomembr.* **1991**, 1062, 123.
- [35] L. Han, K. Liu, M. Wang, K. Wang, L. Fang, H. Chen, J. Zhou, X. Lu, *Adv. Funct. Mater.* **2018**, 28, 1704195.
- [36] J. Li, W. R. Illeperuma, Z. Suo, J. J. Vlassak, *ACS Macro Lett.* **2014**, 3, 520.
- [37] J. Li, Z. Suo, J. J. Vlassak, *J. Mater. Chem. B* **2014**, 2, 6708.
- [38] C. H. Yang, M. X. Wang, H. Haider, J. H. Yang, J.-Y. Sun, Y. M. Chen, J. Zhou, Z. Suo, *ACS Appl. Mater. Interfaces* **2013**, 5, 10418.
- [39] A. Miriyev, K. Stack, H. Lipson, *Nat. Commun.* **2017**, 8, 596.
- [40] H. Yang, S. Ji, I. Chaturvedi, H. Xia, T. Wang, G. Chen, L. Pan, C. Wan, D. Qi, Y.-S. Ong, *ACS Mater. Lett.* **2020**, 2, 478.
- [41] H. Liao, X. Guo, P. Wan, G. Yu, *Adv. Funct. Mater.* **2019**, 29, 1904507.
- [42] H. Qiao, P. Qi, X. Zhang, L. Wang, Y. Tan, Z. Luan, Y. Xia, Y. Li, K. Sui, *ACS Appl. Mater. Interfaces* **2019**, 11, 7755.
- [43] S. Cheng, Y. S. Narang, C. Yang, Z. Suo, R. D. Howe, *Adv. Mater. Interfaces* **2019**, 6, 1900985.
- [44] Y. Bai, B. Chen, F. Xiang, J. Zhou, H. Wang, Z. Suo, *Appl. Phys. Lett.* **2014**, 105, 151903.
- [45] J. L. Dashnau, N. V. Nucci, K. A. Sharp, J. M. Vanderkooi, *J. Phys. Chem. B* **2006**, 110, 13670.
- [46] S. Cerveny, J. Colmenero, A. Alegria, *Macromolecules* **2005**, 38, 7056.
- [47] H. Yuk, B. Lu, S. Lin, K. Qu, J. Xu, J. Luo, X. Zhao, *Nat. Commun.* **2020**, 11, 1604.
- [48] L. B. Lane, *Ind. Eng. Chem.* **1925**, 17, 924.
- [49] X. P. Morelle, W. R. Illeperuma, K. Tian, R. Bai, Z. Suo, J. J. Vlassak, *Adv. Mater.* **2018**, 30, 1801541.
- [50] J. Yang, R. Bai, J. Li, C. Yang, X. Yao, Q. Liu, J. J. Vlassak, D. J. Mooney, Z. Suo, *ACS Appl. Mater. Interfaces* **2019**, 11, 24802.
- [51] D. Rus, M. T. Tolley, *Nature* **2015**, 521, 467.
- [52] H. Yuk, T. Zhang, G. A. Parada, X. Liu, X. Zhao, *Nat. Commun.* **2016**, 7, 12028.
- [53] J. Yang, R. Bai, B. Chen, Z. Suo, *Adv. Funct. Mater.* **2020**, 30, 1901693.
- [54] H. Yuk, C. E. Varela, C. S. Nabzdyk, X. Mao, R. F. Padera, E. T. Roche, X. Zhao, *Nature* **2019**, 575, 169.
- [55] K. Chin, T. Hellebrekers, C. Majidi, *Adv. Intell. Syst.* **2020**, 2, 1900171.
- [56] R. L. Truby, M. Wehner, A. K. Grosskopf, D. M. Vogt, S. G. Uzel, R. J. Wood, J. A. Lewis, *Adv. Mater.* **2018**, 30, 1706383.
- [57] T. Yamaguchi, T. Kashiwagi, T. Arie, S. Akita, K. Takei, *Adv. Intell. Syst.* **2019**, 1, 1900018.
- [58] G. M. Taboada, K. Yang, M. J. Pereira, S. S. Liu, Y. Hu, J. M. Karp, N. Artzi, Y. Lee, *Nat. Rev. Mater.* **2020**, 5, 1.

- [59] S. Wang, J. Xu, W. Wang, G.-J. N. Wang, R. Rastak, F. Molina-Lopez, J. W. Chung, S. Niu, V. R. Feig, J. Lopez, *Nature* **2018**, 555, 83.
- [60] Q. Hua, J. Sun, H. Liu, R. Bao, R. Yu, J. Zhai, C. Pan, Z. L. Wang, *Nat. Commun.* **2018**, 9, 1.
- [61] Q. Xu, L. An, M. Yu, S. Wang, *Macromol. Rapid Commun.* **2008**, 29, 390.
- [62] J. Kim, J. R. Sempionatto, S. Imani, M. C. Hartel, A. Barfidokht, G. Tang, A. S. Campbell, P. P. Mercier, J. Wang, *Adv. Sci.* **2018**, 5, 1800880.
- [63] X. Pu, M. Liu, X. Chen, J. Sun, C. Du, Y. Zhang, J. Zhai, W. Hu, Z. L. Wang, *Sci. Adv.* **2017**, 3, e1700015.
- [64] F. Ilievski, A. D. Mazzeo, R. F. Shepherd, X. Chen, G. M. Whitesides, *Angew. Chem., Int. Ed.* **2011**, 50, 1890.
- [65] R. F. Shepherd, F. Ilievski, W. Choi, S. A. Morin, A. A. Stokes, A. D. Mazzeo, X. Chen, M. Wang, G. M. Whitesides, *Proc. Natl. Acad. Sci. USA* **2011**, 108, 20400.
- [66] W. Xie, J. Duan, H. Wang, J. Li, R. Liu, B. Yu, S. Liu, J. Zhou, *J. Mater. Chem. A* **2018**, 6, 24114.
- [67] Q. Rong, W. Lei, J. Huang, M. Liu, *Adv. Energy Mater.* **2018**, 8, 1801967.
- [68] Y. Ren, J. Guo, Z. Liu, Z. Sun, Y. Wu, L. Liu, F. Yan, *Sci. Adv.* **2019**, 5, eaax0648.
- [69] J. Xu, G. Wang, Y. Wu, X. Ren, G. Gao, *ACS Appl. Mater. Interfaces* **2019**, 11, 25613.
- [70] Y. Yang, L. Guan, X. Li, Z. Gao, X. Ren, G. Gao, *ACS Appl. Mater. Interfaces* **2019**, 11, 3428.
- [71] Q. Rong, W. Lei, L. Chen, Y. Yin, J. Zhou, M. Liu, *Angew. Chem., Int. Ed. Engl.* **2017**, 56, 14159.
- [72] Z. Qin, D. Dong, M. Yao, Q. Yu, X. Sun, Q. Guo, H. Zhang, F. Yao, J. Li, *ACS Appl. Mater. Interfaces* **2019**, 11, 21184.
- [73] S. Li, H. Pan, Y. Wang, J. Sun, *J. Mater. Chem. A* **2020**, 8, 3667.
- [74] J. Song, S. Chen, L. Sun, Y. Guo, L. Zhang, S. Wang, H. Xuan, Q. Guan, Z. You, *Adv. Mater.* **2020**, 32, 1906994.
- [75] Z. Liu, Y. Wang, Y. Ren, G. Jin, C. Zhang, W. Chen, F. Yan, *Mater. Horiz.* **2020**, 7, 919.
- [76] H. Chen, X. Ren, G. Gao, *ACS Appl. Mater. Interfaces* **2019**, 11, 28336.